PORE STRUCTURE CHARACTERIZATION OF CATALYST SUPPORTS VIA LOW FIELD NMR

D.M. Smith[1], C.L. Glaves[1], D.P. Gallegos[1], C.J. Brinker[2]

[1] UNM CENTER FOR MICRO-ENGINEERED CERAMICS
University of New Mexico
Albuquerque, New Mexico 87131 USA
[2] Division 1846
Sandia National Laboratories
Albuquerque, NM 87185 USA

Two characterization techniques (mercury porosimetry and nitrogen adsorption/condensation) are widely employed for pore structure analysis of catalyst supports. Pore structure analysis is an important component of catalysis at several levels ranging from quality control for catalyst support production to the understanding of mass transfer resistance in laboratory experiments. Although porosimetry and adsorption/condensation are widely used, they suffer from several disadvantages. In an effort to avoid these disadvantages and to extract more detailed pore structure information, techniques such as small-angle x-ray/neutron scattering (SAXS/SANS), phase-change porosimetry, and low-field NMR spin-lattice relaxation measurements have been recently employed. In this paper, the application of low-field NMR to both surface area and pore structure analysis of catalyst supports will be presented. Low-field (20 MHz) spin-lattice relaxation (T_1) experiments are performed on fluids contained in alumina and silica catalyst supports. Pore size distributions (PSD) calculated from these NMR experiments are compared to those obtained from mercury porosimetry and nitrogen condensation.

BACKGROUND - Conventional Pore Structure Characterization

Mercury porosimetry employs the measurement of mercury volume intruded (or retracted) into a sample as a function of pressure. The applied pressure is related to the desired pore size via the Washburn Equation [1] which implies a cylindrical pore shape assumption. Mercury porosimetry is widely applied for catalyst characterization in both QC and research applications for several reasons including rapid reproducible analysis, a wide pore size range (≈2 nm to >100 μm, depending on the pressure range of the instrument), and the ability to obtain specific surface area and pore size distribution information from the same measurement. Accuracy of the method suffers from several factors including contact angle and surface tension uncertainty, pore shape effects, and sample compression. However, the largest discrepancy between a mercury porosimetry-derived pore size distribution (PSD) and the actual PSD usually arises as a result of network/percolation effects. An implicit assumption in porosimetry analysis is that every individual pore is in direct contact with the pellet surface. In fact, a particular pore in a catalyst support will be connected to the surface via a network of various size/shape pores. Mercury will intrude into the pore not at the pressure associated with the size of that specific pore but at a pressure corresponding to the smallest constriction in the largest branch of the network connecting the pore to the surface. This effect will result in the apparent PSD being skewed to smaller pore sizes. When the pressure is lowered, (i.e., retraction), a different pressure will be observed for the same pore as the retraction will occur through the path with the largest constrictions.

Investigators have attempted to model this network problem using percolation theory in an attempt to extract additional pore structure information from the intrusion curve. Using a pore model based on the pore space surrounding random packing of solid monodisperse spheres (a reasonable model for a catalyst support with a monodisperse pore structure or with macropores surrounding a packing of porous microspheres), Mason [2] concluded that only 16% of the pores could be observed as a result of network/percolation effects. Recently, Smith and co-workers [3] refined Mason's work and demonstrated that actually 27% of the pores could be observed with porosimetry but these would primarily be the smaller pores. In an attempt to extract further pore size information, some investigators also employ the depressurization (retraction) curve. For example, Conner and co-workers [4] indicate that pore morphology information may be obtained by comparing the intrusion and extraction curves. This approach seems to work reasonably well for materials with narrow, unimodal pore size distributions. However, Ciftcioglu and co-workers [5] have recently demonstrated that the retraction curve may be dominated by the size of only a few large internal pores and that negligible information concerning the majority of the pores is obtained if the material has a broad distribution with a "well-connected" pore network. In principle, further pore structure information may be obtained by performing repeated scanning curves in the hysterisis region but the additional effort is rarely justified in terms of the additional information obtained.

Nitrogen adsorption/condensation is used for the determination of specific surface areas (relative pressure < 0.3) and pore size

distributions in the pore size range of 1 to 100 nm (relative pressure > 0.3). As with mercury porosimetry, surface area and PSD information are obtained from the same instrument. Typically, the desorption branch of the isotherm is used (which corresponds to the porosimetry intrusion curve). However, if the isotherm does not plateau at high relative pressure, the calculated PSD will be in error. For PSD's, nitrogen condensation suffers from many of the same disadvantages as porosimetry such as network/percolation effects and pore shape effects. In addition, adsorption/condensation analysis can be quite time consuming with analysis times greater than 1 day for PSD's with reasonable resolution.

Despite the shortcomings of these methods, they serve as the principle analytical tools for catalyst support characterization. If one is interested in quality control applications and solely looking for qualitative differences between different batches of the same or similar supports, the errors associated with these methods are minor. However, if one requires detailed structural information, the use of additional and/or more sophisticated techniques is required.

BACKGROUND - Characterization via NMR

The attractiveness of surface/pore characterization via NMR spin-lattice relaxation measurements of pore fluid lies in the potential advantages this technique has as compared to the conventional approaches. These include: rapid analysis, lower operating costs, analysis of wet materials, no pore shape assumption, a wide range of pore sizes can be evaluated (0.5 nm to >1 μm), no network/percolation effects and the technique is non-destructive.

When determining specific surface areas, NMR analysis does not require out-gassing and has the potential for on-line analysis of slurries.

Early studies involving NMR include the work by Hanus and Gillis [6] in which spin-lattice relaxation decay constants were studied as a function of available surface area of colloidal silica suspended in water. Senturia and Robinson [7] and Loren and Robinson [8] used NMR to qualitatively correlate mean pore sizes and observed spin-lattice relaxation times. Schmidt and co-workers [9] have qualitatively measured pore size distributions in sandstones by assuming the value of the surface relaxation time. Brown and co-workers [10] obtained pore size distributions for silica, alumina, and sandstone samples by shifting the T_1 distribution until the best match was obtained between distributions obtained from porosimetry and NMR. More recently, low field (20 MHz) NMR spin-lattice relaxation measurements were successfully demonstrated by Gallegos and co-workers [11] as a method for quantitatively determining pore size distributions using porous media for which the "actual" pore size distribution is known apriori. Davis and co-workers have modified this approach to rapidly determine specific surface areas [12] of powders and porous solids.

THEORY - NMR

The technique is based on the observed decrease in the spin-lattice relaxation decay constant, T_1, of a fluid in contact with a solid surface as compared with the T_1 for the fluid alone. Within this fluid there are assumed to exist two discrete regions: a surface affected region, in which relaxation is fast, and a region

which acts as bulk fluid. If diffusion between the regions is much faster than relaxation, than for a given pore size, a single T_1 will exist and can be described by the "two-fraction, fast-exchange" model [13]. In terms of the hydraulic pore radius, r_p, this governing equation for a saturated porous medium is given as [11]:

$$1/T_1 = \alpha + \beta/r_p \tag{1}$$

where α is the reciprocal bulk fluid T_1 and β is a surface relaxation parameter inversely proportional to the surface phase T_1, and incorporating the surface layer thickness. α may be determined by performing a relaxation experiment on the fluid and is a function of temperature and the fluid. For water at ambient temperature, α is on the order of 0.3-0.5 s^{-1}. β will be a function of fluid, temperature, proton frequency and surface chemistry. For decreasing proton frequency (field strength), β will increase resulting in increased pore sizing sensitivity. Also with decreasing frequency, the signal to noise ratio of the T_1 measurements will decrease implying a decrease in sensitivity. Therefore, the optimum frequency will depend upon both the pore size and pore volume of the sample. For most applications, frequencies in the range of 10 to 60 MHz are satisfactory.

The measured data for a single pore size or a bulk fluid is an exponentially decaying fluid magnetization vector versus time in which T_1 is the decay constant. For a 180°-τ-90° pulse sequence, the return to equilibrium of the magnetization vector is described by:

$$M(\tau) = M_0 \, [1 - 2 \exp(-\tau/T_1)] \tag{2}$$

where M_0 is the magnetization at equilibrium. However, a typical porous media will have a distribution of pore sizes, resulting in a

magnetization curve which receives contributions from each pore size in the form of different T_1's. This implies that the observed magnetization is described by:

$$M(\tau) = M_0 \int_{T_{1min}}^{T_{1max}} [1 - 2 \exp(-\tau/T_1)] \, f(T_1) \, dT_1 \qquad (3)$$

T_{1max} is the maximum expected value of T_1 and is usually taken to be the T_1 for the bulk fluid. T_{1min} is the minimum T_1 value and is usually taken to be equal to the shortest T_1 which can be measured with the particular instrument used. Deconvolution of Equation 3 to yield the desired T_1 distribution has been accomplished via non-negative least squares [14] (discrete distributions) and regularization [15] (continuous distributions) algorithms. The desired pore size distribution can then be determined from the T_1 distribution via the application of Equation 1.

Equation 1 is applicable (i.e., no pore shape assumption) for pores with radius greater than about 5 nm. However, the model has been extended to pores as small as 0.5 nm [16] by assuming a pore shape. In addition, the fraction of pore volume with pore size less than 0.5 nm may be obtained (assuming that the concept of pore size in this size range has physical significance) although distribution information in that region can not be determined.

The value for α can be determined independently but the magnitude of the surface interaction parameter, β, must be found for the particular frequency/fluid/temperature/solid system being studied. Schmidt and co-workers [9] simply assumed a β value. Other workers [10,11] matched the NMR and mercury porosimetry derived pore size distributions to estimate β. More recently, Davis and co-workers [12] have shown that β can be found via a series of T_1

experiments, varying the quantity of fluid sorbed on the solid surface. In that work it was shown that a plot of inverse average T_1 versus the surface area (as determined via conventional methods) times solid concentration (SA*C) will give a line with slope ($\beta/2$) and intercept α. This value of β can then be applied to find unknown surface areas and pore size distributions using experimentally determined T_1's for similar material at the same fluid, frequency and temperature.

EXPERIMENTAL

The pore structure of two types of catalyst support material were studied: γ-alumina and silica aerogel. The alumina samples were commercial catalyst supports made in 1/8 inch diameter pellet form by Harshaw Chemical. Silica aerogels were prepared from silica gels synthesized by a two step acid/base catalyzed procedure employing TEOS with a water to silicon ratio equal to 3.7 [17] and ammonium hydroxide concentration of 0.005 M (sample A) or 0.01 M (sample B). Following gelation, the samples were aged in their respective liquor at 323 K for 3 weeks (sample A) or 2 weeks (sample B). The aged samples were solvent exchanged with CO_2 (at 298 K and 54 atm) and critical point dryed at 313 K and 81.7 atm to produce aerogels. As we will show, the aerogel pore structure is sensitive to the ammonium hydroxide concentration employed in the aging procedure. The pore size distribution of the alumina material was determined via NMR and compared to results obtained by mercury intrusion and nitrogen adsorption/condensation techniques. The pore size distributions of the two aerogel samples were measured via NMR

and nitrogen adsorption/condensation only; the material being too compressible for porosimetry.

NMR spin-lattice relaxation inversion recovery (180^0-τ-90^0) experiments were conducted on the samples using distilled water as the fluid probe. Additional NMR experiments using cyclohexane were performed on the alumina material. NMR experiments were performed using a Spin Lock Ltd. CPS-2 pulse NMR at a frequency of 20 MHz and temperature of 303 K. Relaxation curves were obtained by measuring the FID at approximately 30 different τ values between 10 μs and 9 s. Samples for NMR experiments were saturated via a number of techniques. For full saturation, the alumina samples were immersed in the fluid of interest, whereas the aerogel samples were allowed to equilibrate with vapor introduced after evacuating the samples to approximately 5 Pa. Partial saturation was accomplished by evacuating the samples and then allowing them to equilibrate with vapor over salt solutions. Fluid uptake was determined gravimetrically.

Nitrogen adsorption/condensation measurements were performed using an Autosorb-1 analyzer to calculate sample surface area and pore size distribution. BET analysis at 77 K was applied for extracting the monolayer capacity from the adsorption isotherm and a N_2 molecular cross-sectional area of 0.162 nm^2 was used to relate the monolayer capacity to surface area. PSD's were calculated from the desorption branches of the isotherms using a modified form of the BJH method [18]. Mercury intrusion measurements were performed using an Autoscan-33 continuous scanning mercury porosimeter (12-33000 psia) and a contact angle of 140°.

RESULTS

Sample pore volumes and surface areas via nitrogen adsorption/condensation and mercury intrusion are given in Table 1. For the alumina sample, the total pore volumes obtained from condensation and mercury intrusion are in reasonable agreement. The larger value from mercury may be the result of sample compression and/or the presence of pores ≈70 nm (i.e., corresponding to the largest relative pressure used). For the silica aerogels, pore volumes could not be obtained by porosimetry because sample compression effects dominated the observed intrusion (based on the observation that no mercury was extracted from the samples on the depressurization curve and visual inspection of the sample before and after analysis). For the sample B aerogel, nitrogen adsorption indicated the presence of a small amount of microporosity.

Magnetic data from the NMR spin-lattice relaxation experiments on fully saturated samples were deconvoluted into continuous T_1 distributions via the regularization algorithm. NMR experiments at different saturation levels were used to obtain the α and β parameters which relate the T_1 distributions to pore size distributions (eq 1.) Figure 1 is a plot showing the result of these partial saturation experiments for water, with the inverse average T_1 (obtained from NNLS) plotted vs. the surface area multiplied by the solid concentration. The partial saturation experiments for water exhibited single T_1 decay. The slope and intercept of the lines in Figure 1 were used to calculate β and α respectively.

Cyclohexane was also used as a fluid for the alumina pellets. When partial saturation NMR experiments were performed using cyclohexane, the resulting T_1 distributions were very broad, making a

plot similar to those in Figure 1 impossible to construct. It is believed that the partial saturation experiments using cyclohexane were not appropriate for the alumina material because of the large size of the cyclohexane molecule compared to the average pore size. α and β were instead calculated for the alumina/cyclohexane system via a one-point method, i.e. taking α to be the inverse of the T_1 for bulk cyclohexane and calculating β from the average T_1 of the fully saturated sample (a single T_1 decay) using:

$$1/T_1 = \alpha + \beta/2 \text{ SA} * C \qquad (4)$$

C was determined gravimetrically and SA was taken as the N_2 surface area. α and β values calculated for the various samples are given in Table 2. Partial saturation experiments for the aerogel material were conducted only on sample B. The α and β values obtained were assumed to be the same for sample B which was of similar composition, differing in pore structure only. The validity of this assumption has been demonstrated in other work [12] wherein samples of similar material but different pore structure fit the same straight line on plots of the type shown in Figure 1.

The calculation of NMR pore size distributions is a three step process once the values of α and β are known. First a spin-lattice relaxation experiment is undertaken on a saturated sample and a data set of magnetization-delay time, $M(\tau)$, is obtained. The magnetization data is subsequently deconvoluted using regularization to obtain a distribution of pore volume with T_1. Finally, Equation 1 is applied to convert from T_1 to pore size and obtain the desired pore size distribution. This process is illustrated in Figure 2 for the alumina sample saturated with cyclohexane.

The T_1 distributions of fully saturated samples were combined with the α and β values of Table 2 to produce pore size distributions for each material. The NMR pore size distributions were compared for each type of material to pore size distributions obtained via nitrogen adsorption/condensation (all materials) and mercury porosimetry (alumina samples). The results are shown in Figure 3 for alumina and in Figure 4 for the aerogels. In each case the NMR agrees fairly well with the other techniques, but is seen to result in slightly larger pore sizes. This is consistent with the limitations of the other techniques which generally result in smaller than actual pore size measurements due to constricted pores and network/percolation effects. The NMR results for water and cyclohexane in alumina should agree closely. The difference noted is probably due to inaccuracies in the cyclohexane α and β which had been calculated using a one-point method.

ACKNOWLEDGEMENTS

This work has been supported by Sandia National Laboratories (#55-6778) and the ALCOA Foundation. Nitrogen adsorption and mercury porosimetry measurements were performed by S.B. Ross. Aerogels were prepared by Carol S. Ashley.

REFERENCES

[1] Washburn, E.W.; Phys. Rev., 1921, 17, 273..

[2] Mason, G.; J. Colloid Interface Sci., 1972, 41, 208.

[3] Smith, D.M., Gallegos, D.P., Stermer, D.L.; Powder Tech., 1987, 53, 11.

[4] Conner, W.C., Weist, E.L., Pedersen, L.A.; PREPARATION OF CATALYSTS IV: Delmon, Grange, Jacobs, and Poncelet Editors, Elsevier, Amsterdam, 1987.

[5] Ciftcioglu, M., Smith, D.M., Ross, S.B.; Powder Tech., in press.

[6] Hanus, F., Gillis, P.; J. Mag. Resonance, 1984, 59, 437.

[7] Senturia, S.D., Robinson, J.D.; Soc. Pet. Eng. J., 1970, 10, 237.

[8] Loren, J.D., Robinson, J.D.; Soc. Pet. Eng. J., 1970, 10, 268.

[9] Schmidt, E.J., Velasco, K.K., Nur, A.M.; J.Appl.Phys., 1986, 59, 2788.

[10] Brown, J.A., Brown, L.F., Jackson, J.A., Milewski, J.V., Travis, J.V.; Proceedings of the SPE/DOE Unconventional Gas Recovery Symposium, 1982, 201.

[11] Gallegos, D.P., Munn, K., Smith, D.M., Stermer, D.L.; J. Colloid Interface Sci., 1987, 19, 127.

[12] Davis, P.J., Gallegos, D.P., Smith, D.M.; Powder Tech., 1987, 53, 39.

[13] Brownstein, K.R., Tarr, C.E.; J. Mag. Resonance, 1980, 39, 297.

[14] Munn, K., Smith, D.M.; J. Colloid Interface Sci., 1987, 119, 117.

[15] Gallegos, D.P., Smith, D.M.; J. Colloid Interface Sci., 1988, 122, 143.

[16] Gallegos, D.P., Smith, D.M., Brinker, C.J.; J. Colloid Interface Sci., 1988, 124, 186.

[17] Brinker, C.J., Keefer, K.D., Schaefer, D.W., Ashley, C.S.; J. Non-Crystalline Solids, 1982, 48, 47.

[18] S. Lowell and J. Shields, Powder Surface Area and Porosity; Chapman & Hall: London, 1984.

Table 1. Pore Volume and Surface Area

Sample	Pore Volume (cc/g) Hg	Pore Volume (cc/g) N_2	Surface Area (m^2/g) N_2
Alumina	0.7594	0.7312	235.1
Aerogel A	--	4.34	427.9
Aerogel B	--	4.20	751.3

Table 2. α and β Values

Material	Fluid	$\alpha(s^{-1})$	β(nm/s)
Alumina	Water	1.19	105.5
Alumina	Cyclohexane	0.481	8.28
Aerogel	Water	.566	8.64

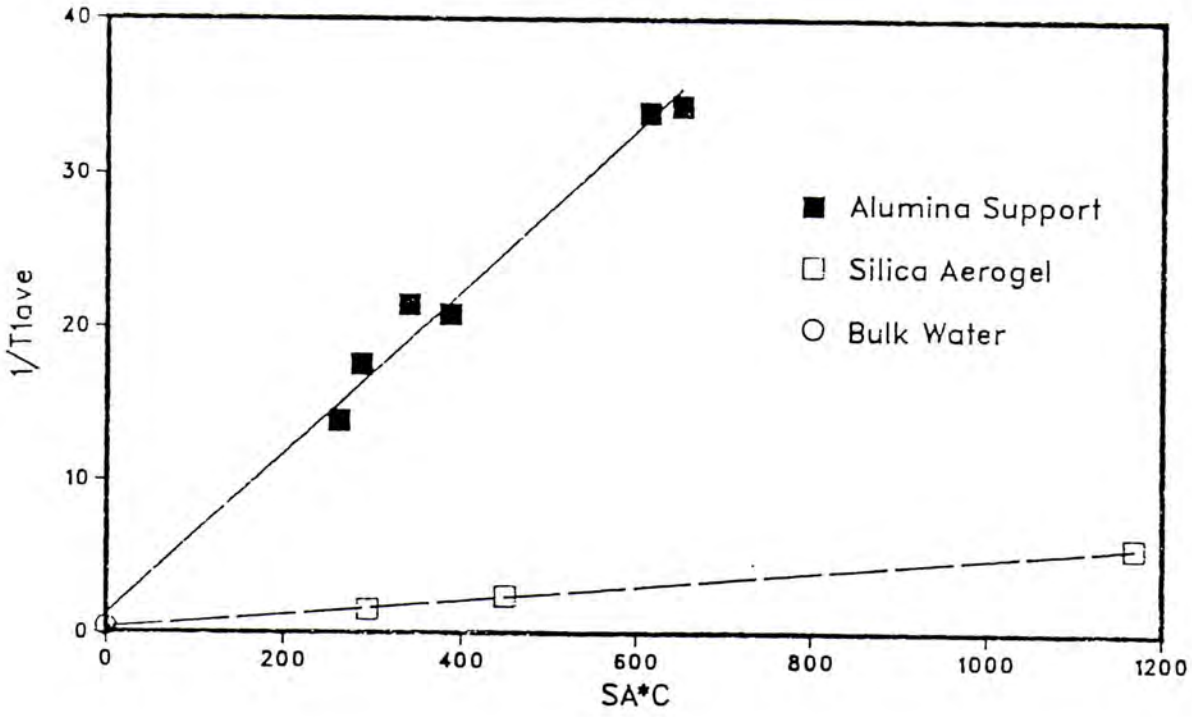

Figure 1 SA*C plots for determination of α and β.

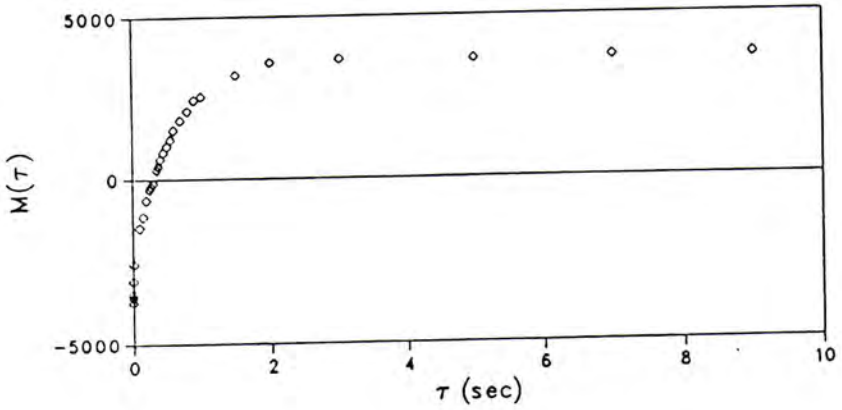

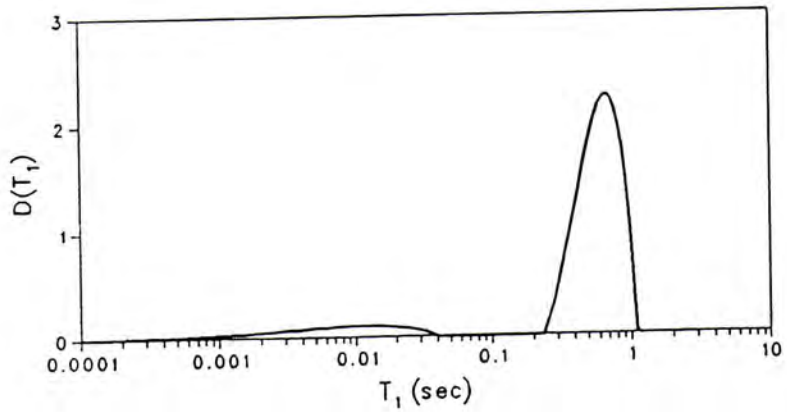

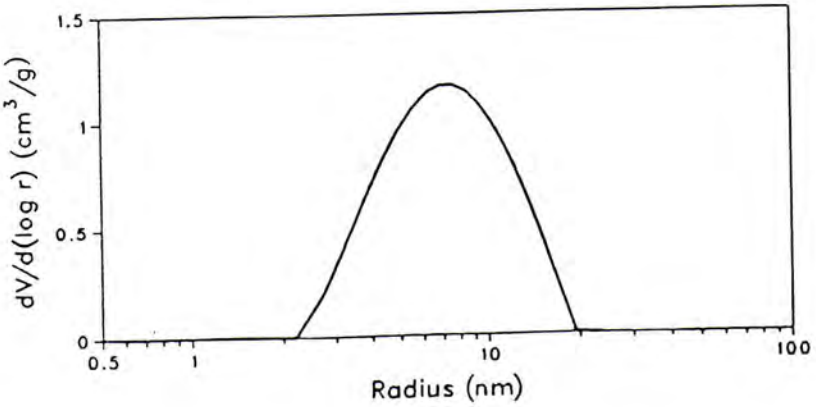

Figure 2 $M(\tau)$, $f(T_1)$ and PSD plots for cyclohexane in alumina.

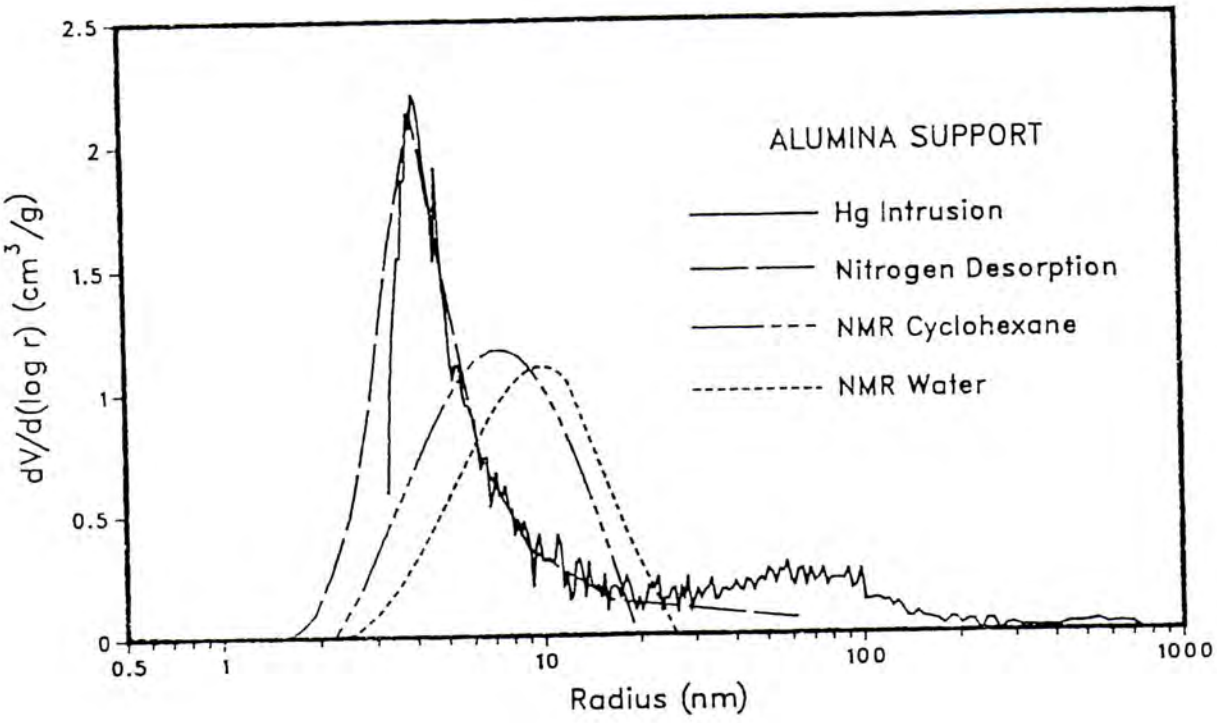

Figure 3 NMR, nitrogen condensation and porosimetry PSD's for alumina.

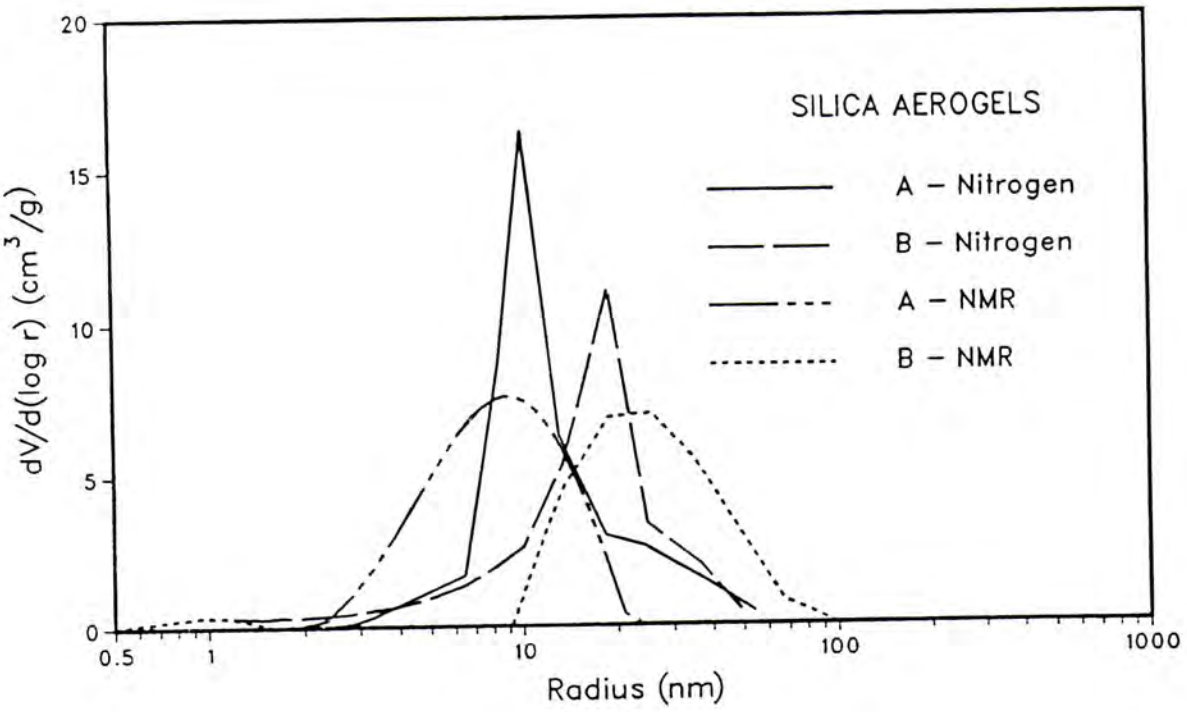

Figure 4 NMR and nitrogen condensation PSD's for silica aerogels.